

See discussions, stats, and author profiles for this publication at: <https://www.researchgate.net/publication/26890277>

Generation and Integration of NaOH into NaCl Clusters in Supercritical Water: A Molecular Dynamics Study on Hydrolysis Product Partitioning

ARTICLE *in* THE JOURNAL OF PHYSICAL CHEMISTRY B · OCTOBER 2009

Impact Factor: 3.3 · DOI: 10.1021/jp9039572 · Source: PubMed

CITATIONS

6

READS

26

2 AUTHORS:



Istok Nahtigal

Bioniche Life Sciences Inc.

6 PUBLICATIONS 61 CITATIONS

[SEE PROFILE](#)



Igor M. Svishchev

Trent University

70 PUBLICATIONS 1,855 CITATIONS

[SEE PROFILE](#)

Generation and Integration of NaOH into NaCl Clusters in Supercritical Water: A Molecular Dynamics Study on Hydrolysis Product Partitioning

Istok G. Nahtigal and Igor M. Svishchev*

Department of Chemistry, Trent University, Peterborough, ON, Canada K9J 7B8

Received: January 23, 2009; Revised Manuscript Received: July 29, 2009

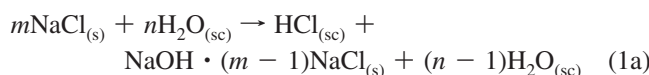
The interaction of water with NaCl nanoparticles at supercritical conditions has been studied by molecular dynamics (MD) simulation. During the nanoparticle nucleation process, water is not only physically adsorbed to the periphery of the NaCl cluster but also exists in a confined state within subsurface regions for several picoseconds. Electrostatic fields generated by the coalescing ions are shown to be on the order of 10^{10} V/m, which can drive the hydrolysis of confined water molecules. A molecular mechanism for the sodium chloride hydrolysis reaction at supercritical conditions is suggested. It involves proton transfer from water to chloride ions, followed by hydrolysis product partitioning. We provide MD results displaying the subsurface hydroxide localization in amorphous NaCl clusters, as well as the partitioning of the HCl into the supercritical water phase.

1. Introduction

The properties of acids and bases control much of the aqueous chemistry of biological, geochemical, and industrial systems. Their behavior at ambient conditions is well characterized, but at high temperatures and pressures, the behaviors of acids, bases, salts, and even the ionization of water are quite different. The power industry has been a large motivator in advancing research in the field of high temperature aqueous chemistry, addressing topics such as corrosion, in efforts to increase the efficiency of the power cycle.^{1,2}

Studies of solutions at hydrothermal conditions are numerous in both experimental and computational aspects; however, few researchers have studied the high temperature hydrolysis of the common salt, NaCl. This reaction is by no means a rare event, evidence of the reaction has been reported in past studies^{3–8} remaining largely unaddressed and, consequently, providing us with ample motivation for this work. The analogous hydrolysis reaction of CaCl₂ with water under supercritical conditions has been experimentally reported as generating significant HCl in the vapor phase.⁹ The calcium bromide hydrolysis reaction, the cornerstone of the Ca–Br cycle, has shown to be a potential option for the large scale hydrothermal production of hydrogen gas from water.¹⁰

The molecular process being examined in this modeling study can be written as



where subscripts (sc) refers to supercritical state and (s) refers to the solid (amorphous) state (salt particle); it involves proton transfer from water to chloride ions followed by the hydrolysis product partitioning. At ambient conditions, the hydrolysis reaction of sodium chloride



is endothermic (and unfavorable) with an enthalpy of about 136 kJ/mol (see refs 3 and 4). At these conditions, hydrogen chloride and sodium hydroxide readily dissociate in water and behave similarly to other strong electrolytes (i.e., neutralize each other). However, they exhibit an increasing tendency to associate at high temperatures and low solution densities.^{11,12} The free energies of individual reactions which occur in the reaction (1a) become negative above 450 °C (see Figure 1). This provides favorable conditions for the high temperature hydrolysis. It is also worthwhile noting that in supercritical water, hydrogen chloride behaves as a much weaker electrolyte than NaCl and NaOH,¹¹ with lesser affinity for the neutralization reaction.

As the information on the underlying mechanistic aspects of high temperature hydrolysis is rather scant, we have employed molecular dynamics (MD) simulations to investigate the nucleation of NaCl nanoparticles in supercritical water and partitioning of the potential hydrolysis products, HCl and NaOH, between the nanoparticles and the supercritical medium. Given that experiments at high temperatures and pressures are challenging and costly to carry out, computer simulations often provide a means to study the behavior of electrolytes and their solutions under these extreme conditions. On the basis of our simulation results, we put forward that salts nucleating from supercritical aqueous solutions form solidlike mixtures of NaCl·NaOH, resulting in the effective removal of hydroxide from the supercritical phase, while leaving hydrogen chloride in the supercritical/vapor phase. Results reveal the preferential partitioning of hydroxide to subsurface locals in amorphous NaCl clusters, the presence of surface-bound hydroxide in NaCl crystallites, and the bonding of water to the cluster surface at cationic sites. Local electrostatic fields generated by the clusters are shown to be on the order of 10^{10} V/m, which can drive the hydrolysis of confined water molecules.

This work has an important practical side. For example, corrosion and particle deposition has been found to occur in supercritical water oxidation (SCWO) reactors,¹³ as well as in the moisture transition regions of hydrothermal power plants,

* Corresponding author. Phone: 705-748-1011 ext. 7063. Fax: 705-748-1625. E-mail: isvishchev@trentu.ca

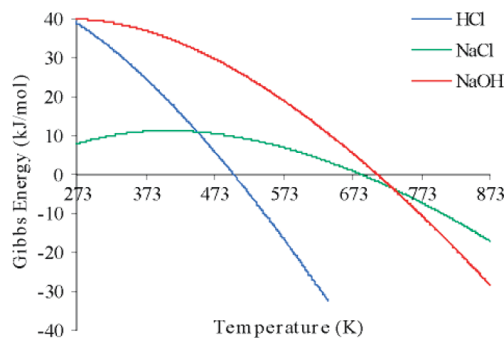


Figure 1. Temperature dependence of the Gibbs energy for the following reactions: (i) $\text{H}_{(\text{aq})}^+ + \text{Cl}_{(\text{aq})}^- \rightarrow \text{HCl}_{(\text{g})}$, (ii) $\text{Na}_{(\text{aq})}^+ + \text{Cl}_{(\text{aq})}^- \rightarrow \text{NaCl}_{(\text{s})}$, (iii) $\text{Na}_{(\text{aq})}^+ + \text{OH}_{(\text{aq})}^- \rightarrow \text{NaOH}_{(\text{s})}$ (Estimates based on ref 4).

even under the relatively stringent guidelines for impurity limits for the feedwater.^{14,15} In order to develop countermeasures to the problems of corrosion and deposition (scale formation), the heterogeneous reactions occurring in nanoparticles require a much better understanding.

The remainder of this paper is organized as follows. In section 2, the modeled reaction process is outlined. Section 3 describes the simulation procedure. Section 4 is devoted to the results of our simulations, while section 5 contains concluding remarks.

2. Reaction Process: General Framework

The bulk properties of water can be attributed to its structure, namely its three-dimensional hydrogen bonded network. When subjected to perturbations, water exhibits structural changes causing changes to its bulk properties. When structurally modified due to its proximity to an ion–solid interface and/or trapped in a confined space, it is often referred to as vicinal or confined water.^{16,17} The common trait to the above environments is the presence of strong electric fields which affect the ability of water to hydrogen bond.

Proton mobility in water has been shown to be abnormally high when compared to all other ionic species, indicating that normal ionic diffusion plays a minor role.^{18,19} One popular theory describing this proton mobility is the Grötthus chain mechanism.^{20,21} Onsanger suggested that H-bonded water chains serve as H^+/OH^- transfer channels.²² The formation of hydroxide and hydronium is greatest when bonding between water molecules is strongest, increasing the Grötthus rate of transfer.

Smaller cations possess high surface charge density and strongly associate with water molecules by virtue of ion–dipole interactions, which are found to become partially covalent through charge redistribution.^{23,24} For the ion–water system under investigation, we adopt (and examine within present simulation) a simplistic reaction scheme that focuses solely on the transfer of a classical proton between a sodium bound water molecule and an H-bonded chloride ion. The proton in this hydrogen bond can be thought of as residing in a double-well potential, one side associated with the donor (H_2O) and the other with the acceptor (Cl^-). The barrier separating the two wells becomes lower as the donor and acceptor come closer, eventually leading to a configuration which results in a symmetric potential, with the hydrogen belonging to either of the two. This treatment of a proton transfer is similar to many other previous studies (see, for instance, the works by Ando and Hynes²⁵ and Bondarenko²⁶).

The charge carrier in this case is the proton and the driving force is the high electrostatic potential acting along the direction of the OH bond of the water molecule (see Figure 2). This

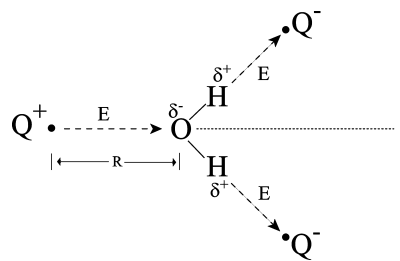


Figure 2. Ion–dipole interaction. The ions have a radial electric field component (\mathbf{E}) which is parallel to the dipole moment vectors. An idealized arrangement of point charges around a central water molecule trapped in the interior of an ionic cluster is shown.

potential drives a concerted one step reaction where the proton is translocated from the water to the chloride, leaving a tightly bound Na^+OH^- ion pair and a weakly interacting (with it) HCl molecule (in this classical picture, the hydroxide ion has a higher affinity toward sodium as compared to HCl, purely based on the molecular and ionic charge distributions). What is essential in our case is that the dynamics of the cluster, where this charge transfer occurs, prevents the recombination of the original species through reverse reaction (neutralization). The high affinity of OH^- toward Na^+ results in rapid formation of a tightly bound shell of sodium ions in the cluster around the hydroxide, essentially preventing any further events where the hydroxide ion can be employed as an H-bond acceptor to water or HCl.

Hydrogen bond dynamics of water solvated anions has been studied by Chandra and co-workers²⁷ at both ambient and supercritical conditions. They report chloride–water lifetimes to be on the order of 2.4 ps at ambient and 0.23 ps at supercritical temperatures. Experimental studies by Kropman and Bakker²⁸ show that a water–chloride oscillator has a vibrational lifetime of 2.6 ps at ambient conditions, whereas the H-bond between two water molecules has a characteristic time of only 0.8 ps. Our earlier studies show that water molecules confined to core regions of ionic clusters (formed in supercritical water) have residence times of 15 ps and higher.^{29,30} These residence times are appreciably longer than for water molecules found in ion hydration shells. Considering that the water molecule has a number of vibrational modes with periods ranging from 9 to 20 fs,³¹ it can undergo approximately 1000 intramolecular motions during its confinement time in the ionic cluster (where it experiences very strong local electric field). Molecules under the influence of external fields undergo changes in their bonds, which are experimentally detectable as vibrational Stark shifts.^{32,33} In our case, these perturbations increase the probability of the system converting from a reactant configuration ($\text{Na}^+\text{--OH}_2^-\text{Cl}^-$) to a product configuration ($\text{Na}^+\text{OH}^-\text{--HCl}$), by inducing proton translocation within the electrostatically “excited” complex.

Density functional calculations on the reaction of water with small NaCl clusters performed by Barnett et al.⁸ indicate the existence of an exothermic reaction yielding diatomic hydrogen and endothermic reactions yielding HCl. It should be noted that experimental studies have reported HCl generation through the reaction (1a) only when appropriate conditions are met.^{5–7} The conditions are somewhat varied between the studies, but low pressures and temperatures above 450 °C appear to be the consensus. Note that at temperatures above 450 °C the individual reactions which occur in the process of hydrolysis become favorable (see Figure 1). Interestingly, this temperature also coincides with the vapor–liquid to vapor–solid transition region on the NaCl– H_2O phase diagram.³⁴

TABLE 1: Dipole Moments and Polarizabilities of Species Simulated

ion/molecule	dipole moment μ (C·m) ³⁷	polarizability α (C ² ·m ² ·J ⁻¹) ³⁷
H ₂ O (SPC/E)	7.84209×10^{-30}	
H ₂ O (real liquid)	8.33910×10^{-30}	
H ₂ O (real gas)	6.18755×10^{-30}	1.6623×10^{-40}
HCl	3.60249×10^{-30}	2.930×10^{-40}
Na ⁺		1.99164×10^{-40}
Cl ⁻		4.0723×10^{-40}

3. Computational Procedure

i. Electrostatics. In this section, we describe the basic equations^{35,36} used in the determination of electric fields within ionic clusters. Conventionally, ions and/or nuclei of a molecule are considered as point charges, and the electrons, as a continuous charge distribution. In the presence of an external perturbation (electric field), atoms and molecules experience distortion of their electron cloud, effectively separating the origins of positive and negative charge. This affects the total dipole moment by creating an induced dipole moment:

$$\mu_{\text{ind}} = \alpha E + \frac{1}{2} \beta E^2 \dots \quad (2)$$

where E is the external electric field, and α and β are the polarizability and hyperpolarizability, respectively. Considering that the dipole moment is proportional to the separation δ between two point charges, q ,

$$\mu = q\delta \quad (3)$$

one can then obtain the separation between the charges based on the resulting “new” dipole moment. To simplify eqs 2 and 3, one can ignore hyperpolarizability, writing the following:

$$\delta = (\mu_{\text{perm}} + \alpha E) q^{-1} \quad (4)$$

The dipole moment and polarizability values for our species are listed in Table 1. In this work, effective rigid (point charge) models for water and ions are employed.

When molecules are free to orient themselves in the presence of an electric field, they will align so that vectors μ and E are parallel in order to occupy the lowest energy orientation. The common notation for electric fields states that for charge $Q > 0$ the field points away from the charge and for $Q < 0$ the field points toward the charge. As an illustration, Figure 2 represents an idealized arrangement of point charges around a central water molecule trapped in the interior of an ionic cluster. The Coulomb force along the dipole axis (z) of the water molecule is

$$F_z = \mu \frac{\partial E}{\partial R} \quad (5)$$

where the electric field \mathbf{E} of the ion has a magnitude of

$$|E| = \frac{Q}{4\pi\epsilon_0 R^2} \quad (6)$$

(In eqs 5 and 6, Q and R are, respectively, charge and separation and ϵ_0 is the permittivity of free space).

TABLE 2: Lennard-Jones Interaction Parameters and Site Charges Used in Simulations

atom	ϵ (kJ/mol)	σ (nm)	q (eps)	ref
O _w	0.65000	0.3166	-0.8476	36
H _w	0.00000	0.0000	0.4238	
Na ⁺	0.54431	0.2350	1.0000	38
Cl ⁻	0.41870	0.4400	-1.0000	
O _{OH}	0.63200	0.3233	-1.3000	39
H _{OH}	0.23100	0.2083	0.3000	
Cl _{HCl}	0.56600	0.4062	-0.1800	40
H _{HCl}	0.00000	0.0000	0.1800	

Computing the local electric fields for the distribution of point charges requires the use of Gauss’ law³⁶

$$\nabla \cdot \mathbf{E} = 4\pi\rho \quad (7)$$

where ρ is the charge density. In eq 7, the electric field is derived from a scalar by the gradient operation. This scalar can be defined as the electrostatic potential Φ and can be computed in the simulation from the distribution of point charges as follows:

$$\Phi(x, y, z) = \sum_i \frac{q_i}{4\pi\epsilon_0} \frac{1}{\sqrt{(x - x_i)^2 + (y - y_i)^2 + (z - z_i)^2}} \quad (8)$$

where $\{x, y, z\}$ are points of interest and $\{x_i, y_i, z_i\}$ are locations of the charge. The electric field strength is then calculated as the negative gradient of the electrostatic potential,³⁵

$$\mathbf{E} = -\nabla\Phi \quad (9)$$

Overall, differential eqs 7–9 describe the behavior of an electrostatic field and can be combined into one partial differential, the Poisson equation:

$$\nabla^2\Phi = -4\pi\rho \quad (10)$$

which satisfies the Laplace equation ($\nabla^2\Phi = 0$) in regions where there is no charge density.

ii. MD Simulation Details. Conditions have been chosen that correspond to ones found in high pressure turbines of typical coal-fired, supercritical water-cooled generating stations. The conditions at the inlet and outlet of the turbine are 450 °C, 30 MPa and 450 °C, 5 MPa, respectively. During the expansion process the system density rapidly decreases, generating tur-

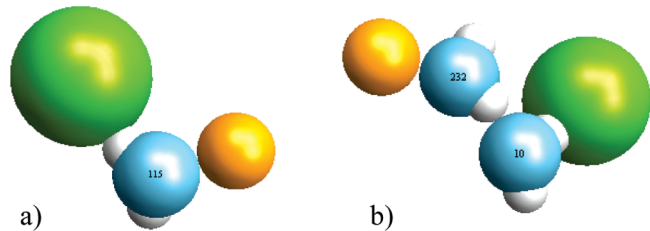


Figure 3. Commonly occurring water–ion configurations which persist for tens of picoseconds within core regions of the nucleating NaCl cluster. Chlorides (green spheres) shown are surface bound whereas the sodiums (orange spheres) are subsurface. (a) Single water configuration. (b) H-bonded configuration. The arrangement seen in part b tends to be rare, whereas the arrangement in part a is very common during the condensation of small clusters.

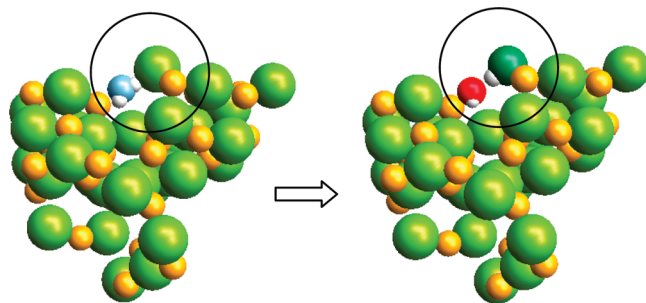


Figure 4. Amorphous cluster with water molecule of interest. Moving from left to right, $\text{Na}^+ \cdots \text{OH}_{2(\text{sc})} \cdots \text{Cl}^-$ transforms to $\text{Na}^+ \cdots \text{OH}^- \cdots \text{HCl}_{(\text{g})}$ where blue is water, red is OH^- , and emerald green is HCl , with white representing hydrogens.

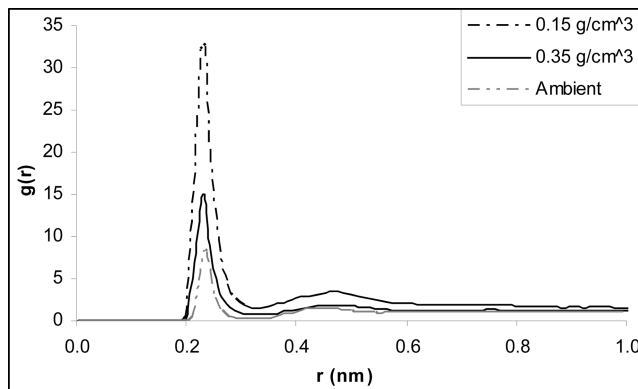


Figure 5. $\text{Na}^+ - \text{O}_w$ radial distribution for low and high pressure supercritical systems ($P = 15$ and 25 MPa and $T = 723$ K) and for ambient pressure and temperature. The ion–water coordination numbers are 4.8, 4.9, and 5.8, respectively.

bulent regions and stimulating and/or accelerating salt nucleation in these areas. Studies involving the salt nucleation process at supercritical water conditions, conducted by Svirshchev et al.^{29,30} have shown that this process has high density dependence.

Simulations are performed in a cubic box containing 400 water molecules and 32 Na^+Cl^- pairs, resulting in a working salt concentration of 20.5 wt %. We must stress that the salt concentrations in this study are purposely above the set impurity limit for heat transfer and coolant feedwater used in power generation. Although, concentrations at this level are not uncommon in the supercritical water oxidation (SCWO) process where most of the liquid effluents to be processed are untreated and rich in mineral salts¹³ or arise as the products of the oxidation process. Our reasons for selecting this concentration are (i) simulations at the impurity limit would require a large amount of computational power and time, (ii) increased particulate build up in stagnant regions, in the vicinity of existing precipitates and near surface crevices, can give rise to high salt concentrations.

The isobaric–isothermal (NPT) ensemble is used in order to imitate the density fluctuations that exist within the heat transfer and/or moisture transition regions. Temperature and pressure are controlled via the Gaussian isokinetic thermostat and the Parrinello–Rahman barostat, respectively, while maintaining a constant number of components. Initial randomized configurations were equilibrated for 0.5 ns and long-range forces were computed by the Ewald summation technique. Four state points were examined, at 30, 25, 15, and 5 MPa, with four independent runs for each of the state points, totaling sixteen runs. Within each of the runs, there were numerous instances where the chosen criteria (below) for proton transfer from H_2O to Cl^- were

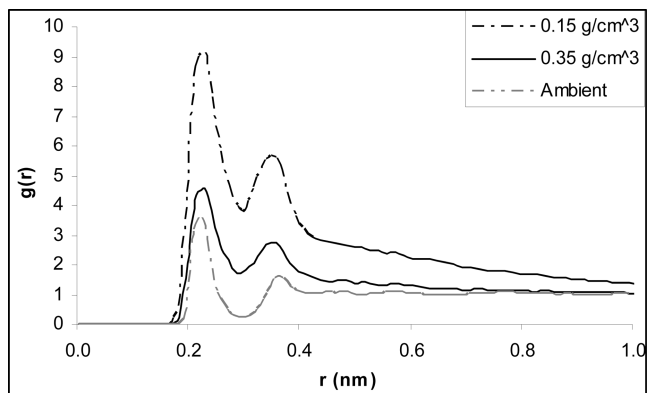


Figure 6. $\text{Cl}^- - \text{H}_w$ radial distribution for low and high pressure supercritical systems ($P = 15$ and 25 MPa and $T = 723$ K) and for ambient pressure and temperature. The ion–water coordination numbers are 5.0, 5.0, and 7.1, respectively.

met. These instances have given us a statistical sample from which to provide an estimate of the field strengths involved (Figure 13 in section 4).

We have opted to use the SPC/E³⁸ water model alongside the sodium and chloride ion parameters from Smith and Dang³⁹ as they have proven to work successfully, at both ambient and supercritical conditions. Our choice of the hydroxide model by Weiner et al.⁴⁰ and the HCl model from Field et al.⁴¹ is likewise based on their past application at supercritical conditions. Interaction parameters for these models are summarized in Table 2. Interaction energies have been calculated based on the two body site–site interaction in the form of the Coulomb plus Lennard-Jones potential:

$$V_{ij} = \sum_{i=1,j=1}^n \frac{1}{4\pi\epsilon_0} \frac{q_i q_j}{r_{ij}} + 4\epsilon_{ij} \left[\left(\frac{\sigma_{ij}}{r_{ij}} \right)^{12} - \left(\frac{\sigma_{ij}}{r_{ij}} \right)^6 \right] \quad (11)$$

The Lorentz–Berthelot mixing rules were applied for cross terms:

$$\sigma_{ij} = \frac{\sigma_i + \sigma_j}{2} \quad \text{and} \quad \epsilon_{ij} = \sqrt{\epsilon_i \epsilon_j} \quad (12)$$

In simple molecular force fields, the charges are held constant and thus cannot change in response to the electrostatic field perturbations induced by the movement of species during the simulation. Molecular and/or ionic electronic structure can be strongly influenced by the surrounding environment,³⁶ leading to hyperpolarizability and quantum mechanical effects; however, since it is not the goal of this work to provide a detailed mechanism of transition states and energy landscapes, the extra computational effort involved in including the aforementioned effects is therefore not warranted at this time.

Proton hydration has proven to be particularly difficult to characterize both experimentally and through simulation, due to the formation of several different hydrated complexes.^{42,43} For this reason, the approach adopted has been to treat the associated and dissociated states of water as distinct. Under the conditions of this study, protons exist primarily as part of a molecule rather than the free entity; thus we employ water (H_2O), hydroxide (OH^-), and hydrogen chloride (HCl) as the constituent molecules. This selection of species is supported by the work of Chialvo et al.,⁴⁴ where they find that at near-critical and supercritical conditions, 97% of $\text{H}_3\text{O}^+ \cdot \text{Cl}^-$ ion pairs

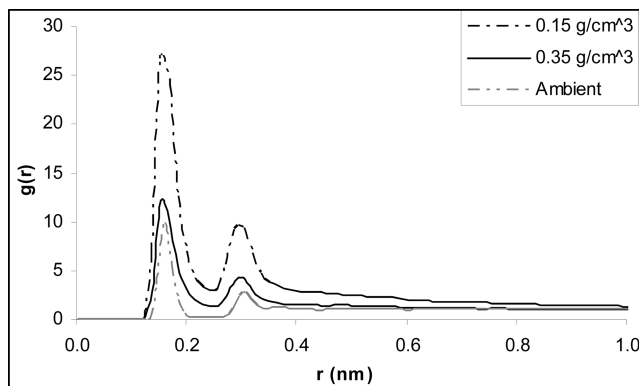


Figure 7. $\text{O}_{\text{OH}}-\text{H}_w$ radial distribution for low and high pressure supercritical systems ($P = 15$ and 25 MPa and $T = 723$ K) and for ambient pressure and temperature. The ion–water coordination numbers are 2.5 , 2.7 , and 3.0 , respectively.

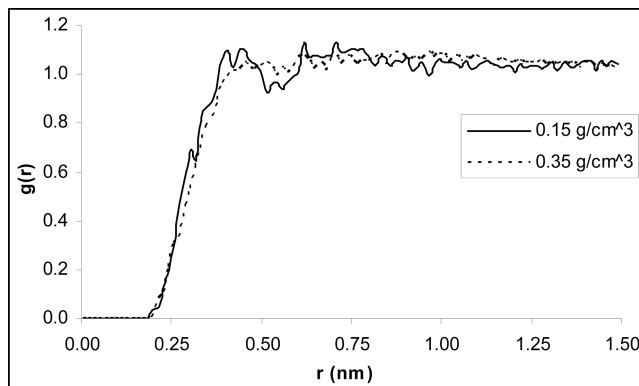


Figure 8. $\text{Cl}_{\text{HCl}}-\text{H}_w$ radial distribution for low and high pressure supercritical systems ($P = 15$ and 25 MPa and $T = 723$ K). The lower pressure result shows a minimum with two water molecules weakly associated.

exist as contact ion pairs. Presumably, they will partition to the vapor phase of our heterogeneous system as HCl. Experimental heat of dilution studies by Holmes et al.⁴⁵ also indicate that the association of hydrogen chloride at temperatures above 250 °C is quite significant.

The criteria used to transform a water molecule (H_2O) and a chloride (Cl^-) to OH^- and HCl are as follows. By examining

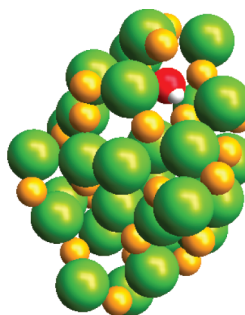


Figure 10. Amorphous NaCl cluster with hydroxide localized to subsurface regions.

simulation trajectory of a nucleating NaCl cluster, we select molecular configurations which have ion–water complexes ($\text{Na}^+ \cdots \text{OH}_2 \cdots \text{Cl}^-$) contained to core regions of a cluster, exhibiting sodium–oxygen and hydrogen–chlorine separations equal to or less than the separations of the first maxima of the radial distribution functions for the sodium–oxygen and hydrogen–chlorine pairs. Figure 3 shows the most commonly occurring configurations matching the above criteria. Figure 4 is a trajectory snapshot matching our prescribed criteria. Then, the appropriate species substitutions are made ($\text{Na}^+ \cdots \text{OH}_2 \cdots \text{Cl}^-$ is transformed to $\text{Na}^+ \cdots \text{OH}^- \cdots \text{HCl}$), and this new molecular configuration is used as the starting configuration from which the MD simulation continues for 0.5 ns. After this second phase of the simulation run, we inspect the resulting cluster configurations and vapor composition, generate the electrostatic potential (ESP) iso-surfaces, and compute select pair-distribution functions.

4. Results and Discussion

i. Solute–Water Pair Distribution Functions. The radial distribution functions (RDFs) represent the average distribution of one species around another. RDF plots of Na^+-O_w , Cl^--H_w , $\text{O}_{\text{OH}}-\text{H}_w$, and $\text{Cl}_{\text{HCl}}-\text{O}_w$ are shown in Figures 5–8, respectively, with results comparing well with other works at similar conditions.^{46–49} Separations between confined water molecules and ions normally do not coincide with the RDF averages (maxima positions). The analysis of select $\text{Na}^+ \cdots \text{OH}_2 \cdots \text{Cl}^-$ configurations within the clusters reveals separations which are

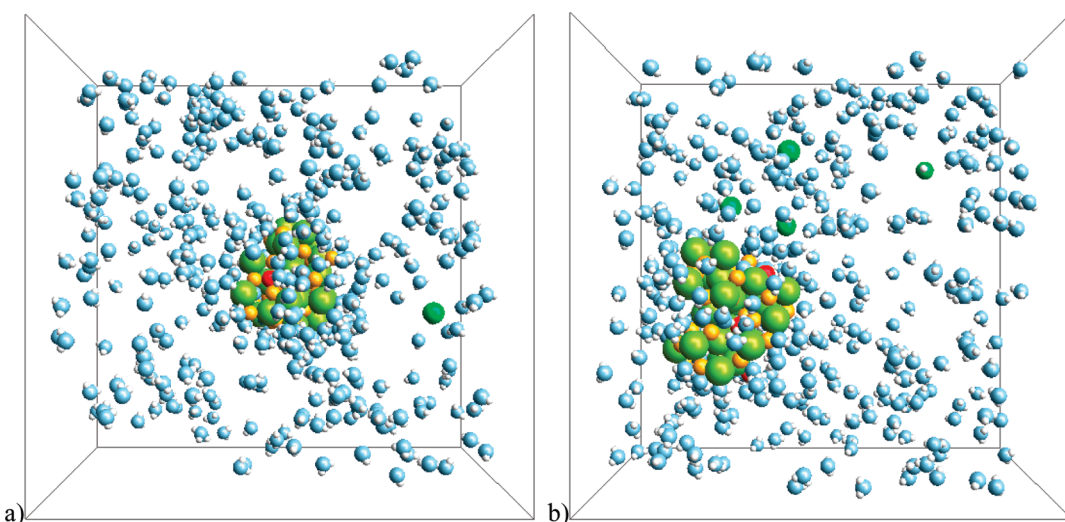


Figure 9. Screen shots of a simulation cell at 230 ps at 15 MPa and 723 K. (a) Simulation with 1 OH^- and 1 HCl . (b) Simulation with 4 OH^- and 4 HCl . Points of interest common to both conditions are the lack of any association of HCl to the NaCl cluster and the amorphicity of the NaCl cluster containing subsurface hydroxide.

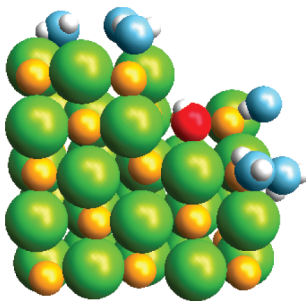


Figure 11. Crystal-like NaCl particle in a low pressure (5 MPa) system. Surface bound water is localized to sodium sites, and the hydroxide is found in an anion site on the surface of the particle.

smaller than the average ion–water separations for the system, indicative of compressive stress on the confined water by the surrounding ions of the nucleating cluster.

ii. Distribution of Species. At ambient conditions $\text{HCl}_{(\text{aq})}$ and $\text{NaOH}_{(\text{aq})}$ behave as a strong acid and base, respectively; however, at elevated temperatures and pressures, they are classified as weak. In Figure 9, we show screen shots of the simulation cell at different conditions, the coloring scheme is described in the caption. Two sets of simulations were performed, with three independent runs at low OH^-/HCl concentration (with 1 OH^- and 1 HCl) and at high concentration (with 4 OH^- and 4 HCl). These extensive simulations were done to validate that the observed partitioning effect was real and not a simulation artifact. In all cases, HCl was observed to be in the supercritical phase and the hydroxide ion as being incorporated into the amorphous NaCl cluster. We may conclude at this point that the hydroxide tends to dissolve in the cluster rather than remain as an ion in the supercritical/vapor phase, which effectively removes it from this phase. This prevents acid–base neutralization from occurring at these conditions.

We now would like to comment on the relationship between local structure of the salt clusters and medium effects. It is known that the nucleating clusters at hydrothermal conditions have a propensity to be amorphous and hydrated.^{29,30} Molecular dynamics simulations in the past have revealed that small ions and large ions associate differently, with the larger ions preferentially existing at interfaces.^{50–53} The ionic radius of the hydroxide ion is smaller than that of the chloride ion, thus hydroxide favors subsurface regions in the cluster, whereas the interface/surface is found to be chloride rich, examples of this can be seen in Figure 10.

As the solution density decreases, the cluster begins to lose its hydrating molecules, enabling crystallization (as observed in this work for the state points at low pressure, see Figure 11). The presence of the hydroxide ion is unfavorable, preventing the cubic ordering of NaCl. Movement of the hydroxide to the surface is energetically favorable, where the hydrogen of hydroxide does not interfere with neighboring sodium ions. These observations are consistent with an experimental study reporting infrared absorptions of hydroxide located at anionic sites of NaCl surfaces.³ The hydroxide ion is known to be a weak hydrogen bond donor and strong acceptor. Considering that the acceptor sites are buried in the crystal, there is little to no water binding to OH^- , as seen in Figure 11.

iii. Electric Fields Involved in Reaction. In the fully ionic interior of salt clusters, the formation of radicals is unlikely (ionic species being the more favorable forms), thus water is expected to dissociate into H^+ and OH^- species. Arguably, dissociation begins when an electric field fluctuation in the cluster is sufficient to cause the polarization and subsequent extension of the oxygen–hydrogen bond, followed by proton transfer, yielding HCl. The dynamical nature of the amorphous cluster spatially separates the hydroxide and HCl so that recombination by the opposite process becomes unfavorable and tends not to occur.

In this work, we have computed electrostatic potential (ESP) maps for the clusters under investigation. As an example, let us refer to Figure 12, where a typical cluster configuration is shown (left image), with water molecule trapped in between an anion and cation separated by 2.614 Å. The electrostatic potential of sodium and chloride ions acting upon trapped water can be extracted from the ESP maps (with an example shown on the right of Figure 12), yielding an average field strength of about 4.22 V/Å, for that specific configuration. To provide a better appreciation of reaction conditions in clusters, in Figure 13, we provide a distribution (histogram) of field strengths acting on confined water molecules collected from thirty two sampled configurations.

iv. Discussion. Molecules in intense electric fields experience large polarizations of their electron clouds. These polarizations, arguably, can result in charge separations which can potentially lead to proton transfers. Charge separation is common in organic molecules, playing important roles in a variety of reactions and more importantly being the underlying process of enzyme activity.

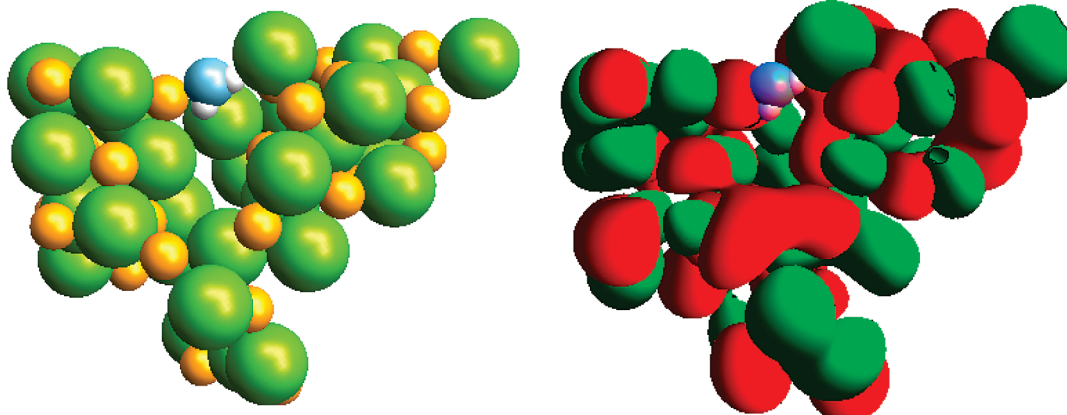


Figure 12. NaCl cluster represented by atomic configuration (left) and electrostatic potential (ESP) contour plot (right). Note the delocalized charge distribution in amorphous regions and localized distribution in crystal-like regions. A contour level has been chosen representing an ESP isosurface value of 5.5 V. Red regions represent areas of positive charge density, whereas green regions are negative charge density.

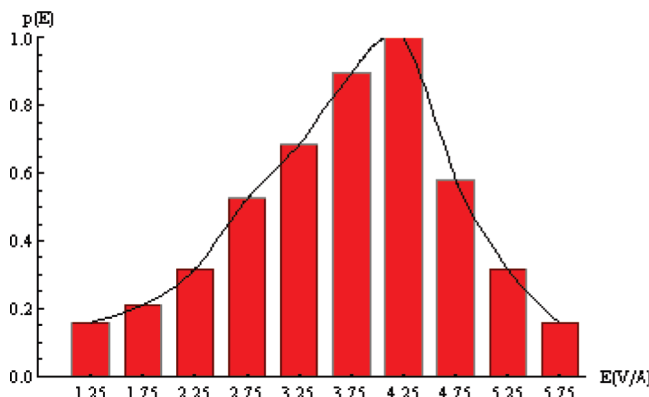


Figure 13. Distribution of electrostatic field values exerted on confined water molecules.

During the ion nucleation process in the SCW, the salt nanoparticle appears as an amorphous cluster with rapid collective dynamics altering the local charge distributions on a continuous basis. This continual rearrangement process ensues up until the point where the cluster becomes crystalline. At this point the internal dynamics and diffusion become arrested; however, some surface (defect) sites retain high mobility and chemical reactivity. In a fashion, salt nuclei formed in SCW can be considered as amorphous salt hydrates. Water molecules are found to occupy voids in these clusters, acting as bridges between cations and anions; an analogous situation is common in low temperature salt hydrate crystals.^{54,55} The dynamic configurations of ions generate enormous electric field effects on trapped water.

On the basis of our simulations, we argue that amorphous cluster hydrates in SCW have the potential to generate local electrostatic fields (see Figure 13, which shows field average of 4.25 V/ \AA) sufficient to dissociate trapped water. Evidence in support of our claim comes from experimental surface-emitter tip studies probing dissociation of water between ice surfaces and Pt electrodes, where breakdown energies of 0.781 V/ \AA have been reported.⁵⁶ Note also, that local fields of 0.5–0.8 V/ \AA have been estimated to exist in the pores of catalytic zeolites,⁵⁷ where water undergoes heterolytic dissociation.

The exact size of the cluster required to induce hydrolysis reaction in SCW is debatable. Experimental studies examining the NaCl driven hydrolysis reaction report that smaller particles tended to promote hydrolysis.⁷ This relates, perhaps, to the internal structures of the salt particles. Larger species tend to be more crystalline having a relatively symmetric patterning of surface fields, except at defect sites. For these larger species, diffusional limitations for the migration of hydroxide ion into the NaCl bulk may also be a contributing factor.

5. Concluding Remarks

Our goal has been to provide molecular level insight into the possibility of NaCl driven hydrolysis reaction and fate of hydroxide and hydrogen chloride, explaining experimentally seen acidic fluid phases and alkaline salt precipitates in hydrothermal systems. We have performed extensive computer simulations at pertinent conditions. We argue that salt nanoclusters formed in supercritical water generate local electrostatic fields necessary to drive the dissociation of trapped water molecules. Local fields generated by the coalescing ions are shown to be on the order of 10^{10} V/m, with the average around 4.25×10^{10} V/m for the sampled configurations. The simulation results show that HCl and NaOH can partition between

coexisting fluid and cluster phases, which nicely explains the presence of acidic condensates and alkaline deposits under hydrothermal conditions. Temperature and pressure play a synergistic role in the process of hydrolysis, driving the kinetics of ion dehydration and determining the extent of ionic association.

In conclusion, we would like to emphasize that similar reactions are likely to play an important role in atmospheric processes and geology.

Acknowledgment. We express our gratitude to the Natural Sciences and Engineering Research Council of Canada and SHARCNET for their financial support. SHARCNET is a consortium of universities and colleges operating a network of high-performance computer clusters across south western, central, and northern Ontario.

References and Notes

- (1) Cengel, Y. A.; Turner, R. H. *Appl. Mech. Rev.* **2004**, *54*, B110.
- (2) Drbal, L. F.; Boston, P. G.; Westra, K. L. *Black and Veatch Power Plant Engineering*; Springer: New York, 1995.
- (3) Dai, D. J.; Peters, S. J.; Ewing, G. E. *J. Phys. Chem.* **1995**, *99*, 10299.
- (4) Atkins, P.; de Paula, J. *Table of Thermodynamic Data*. *Atkin's Physical Chemistry*, eighth ed.; Oxford University Press: New York, 2006.
- (5) Armellini, F. J.; Tester, J. W. *Fluid Phase Equilib.* **1993**, *4*, 123.
- (6) Pitzer, K. S. *Int. J. Thermophys.* **1998**, *19*, 355.
- (7) Hanf, N. W.; Sole, M. J. *Trans. Faraday Soc.* **1970**, *66*, 3065.
- (8) Barnett, R. N.; Landman, U. *J. Phys. Chem.* **1996**, *100*, 13950.
- (9) Bischoff, J. L.; Rosenbauer, R. J.; Fournier, R. O. *Geochim. Cosmochim. Acta* **1996**, *60*, 7.
- (10) Teo, E. D.; Brandon, N. P.; Vos, E.; Kramer, G. J. *Int. J. Hydrogen Energy* **2005**, *30*, 559.
- (11) Ho, P. C.; Palmer, D. A.; Gruszkiewicz, M. S. *J. Phys. Chem. B* **2001**, *105*, 1260.
- (12) Ho, P. C.; Palmer, D. A.; Wood, R. H. *J. Phys. Chem. B* **2000**, *104*, 12084.
- (13) Kritzer, P.; Dinjus, E. *Chem. Eng. J.* **2001**, *83*, 207.
- (14) Ebara, R. *Fatigue Fract. Eng. Mater. Struct.* **2002**, *25*, 855.
- (15) Galobardes, J. F.; Van Hare, D. R.; Rogers, L. B. *J. Chem. Eng. Data* **1981**, *26*, 363.
- (16) Etzler, F. M. *J. Colloid Interface Sci.* **1983**, *92*, 43.
- (17) Brovchenko, I.; Oleinkova, A. *Interfacial and Confined Water*; Elsevier: New York, 2008.
- (18) Bernal, J. D.; Fowler, R. H. *J. Chem. Phys.* **1933**, *1*, 515.
- (19) Miller, I. R. *Biophys. J.* **1987**, *52*, 497.
- (20) Danneel, V. H. Z. *Elektrochim.* **1905**, *11*, 249.
- (21) Agmon, N. *Chem. Phys. Lett.* **1995**, *244*, 456.
- (22) Onsager, L. *Science* **1969**, *166*, 1359.
- (23) Bock, C. W.; Kauffman, A.; Glusker, J. P. *Inorg. Chem.* **1994**, *33*, 419.
- (24) Collins, K. D. *Biophys. J.* **1997**, *72*, 65.
- (25) Ando, K.; Hynes, J. J. *J. Phys. Chem. B* **1997**, *101*, 10464, and references therein. .
- (26) Bondarenko, G. V.; et al. *J. Phys. Chem. A* **2006**, *110*, 4042.
- (27) Mallik, B. S.; Chandra, A. *J. Chem. Phys.* **2006**, *125*, 234502.
- (28) Kropman, M. F.; Bakker, H. J. *Science* **2001**, *291*, 2118.
- (29) Nahtigal, I. G.; Zasetsky, A. Y.; Svishchev, I. M. *J. Phys. Chem. B* **2008**, *112*, 7537.
- (30) Svishchev, I. M.; Zasetsky, A. Y.; Nahtigal, I. G. *J. Phys. Chem. C* **2008**, *112*, 20181.
- (31) Lemus, R. *J. Mol. Spectrosc.* **2004**, *225*, 73.
- (32) González-Férez, R.; Schmelcher, P. *Phys. Rev. A* **2004**, *69*, 023402.
- (33) González-Férez, R.; Schmelcher, P. *Phys. Rev. A* **2005**, *71*, 033416.
- (34) Armellini, F. J.; Tester, J. W. J. *Supercrit. Fluids* **1991**, *4*, 254.
- (35) Berry, R. S.; Rice, S. A.; Ross, J. *Physical Chemistry*, 2nd ed.; Oxford University Press: New York, 2000.
- (36) Jackson, J. D. *Classical Electrodynamics*; John Wiley: Toronto, 1975.
- (37) Lide, D. R. *CRC Handbook of Chemistry and Physics*, 88th ed.; CRC: Boca Raton, FL, 2007.
- (38) Berendsen, H. J. C.; Grigera, J. R.; Straatsma, T. P. *J. Phys. Chem.* **1987**, *91*, 6269.
- (39) Smith, D. E.; Dang, L. X. *J. Chem. Phys.* **1994**, *100*, 3757.
- (40) Weiner, S. J.; Kollman, P. A.; Nguyen, D. T.; Case, D. A. *J. Comput. Chem.* **1986**, *7*, 230.
- (41) Field, M. J.; Bash, P. A.; Karplus, M. *J. Comput. Chem.* **1990**, *11*, 700.

- (42) Tuckerman, M.; Laasonen, K.; Sprik, M.; Parrinello, M. *J. Phys. Chem.* **1995**, *99*, 5749.
- (43) Juanos i Timoneda, J.; Hynes, J. T. *J. Phys. Chem.* **1991**, *95*, 10431.
- (44) Chialvo, A. A.; Ho, P. C.; Palmer, D. A.; Gruszkiewicz, Cummings, P. T.; Simonson, J. M. *J. Phys. Chem.* **2002**, *106*, 2041.
- (45) Holmes, H. F.; Busey, R. H.; Simonson, J. M.; Mesmer, R. E.; Archer, D. G.; Wood, R. H. *J. Chem. Thermodyn.* **1987**, *19*, 863.
- (46) Chialvo, A. A.; Cummings, P. T.; Simonson, J. M. *J. Chem. Phys.* **2000**, *113*, 8093.
- (47) Balbuena, P. B.; Johnston, K. P.; Rossky, P. J. *J. Phys. Chem.* **1996**, *100*, 2706.
- (48) Balbuena, P. B.; Johnston, K. P.; Rossky, P. J. *J. Phys. Chem.* **1996**, *100*, 2716.
- (49) Mucha, M.; Jungwirth, P. *J. Phys. Chem. B* **2003**, *107*, 8271.
- (50) Dang, L. X. *J. Phys. Chem. B* **2002**, *106*, 10388.
- (51) Dang, L. X.; Chang, T. *J. Phys. Chem. B* **2002**, *106*, 235.
- (52) Jungwirth, P.; Tobias, D. J. *J. Phys. Chem. B* **2002**, *106*, 6361.
- (53) Jungwirth, P.; Tobias, D. J. *J. Phys. Chem. B* **2001**, *105*, 10468.
- (54) Ford, T. A.; Falk, M. *J. Mol. Struct.* **1969**, *3*, 445.
- (55) Klewe, B.; Pedersen, B. *Acta Crystallogr. Sect. B* **1974**, *30*, 2363.
- (56) Pinkerton, T. D.; Scovell, D. L.; Johnson, A. L.; Xia, B.; Medvedev, V.; Stuve, E. M. *Langmuir* **1999**, *15*, 851.
- (57) Barrachin, B.; Cohen de Lara, E. *J. Chem. Soc., Faraday Trans. 2* **1986**, *82*, 1953.

JP9039572